Preprints of the 18th IFAC World Congress
Milano (Italy) August 28 - September 2, 2011

Reconfigurable Direct Torque and Flux Control with Torque Ripple Reduction

Matías A. Nacusse* Mónica E. Romero**
Sergio J. Junco ***

* *CONICET – Consejo Nacional de Investigaciones Científicas y Técnicas; Departamento de Control, Facultad de Ciencias Exactas, Ingeniería y Agrimensura, Universidad Nacional de Rosario,*
** *Departamento de Electrónica, Facultad de Ciencias Exactas, Ingeniería y Agrimensura, Universidad Nacional de Rosario,*
*** *Departamento de Control, Facultad de Ciencias Exactas, Ingeniería y Agrimensura, Universidad Nacional de Rosario,*
(e-mail: {nacusse,mromero,sjunco}@fceia.unr.edu.ar)

Abstract: This work presents a reconfigurable direct torque and flux control strategy which guarantees good performance in presence of faults in the actuator, the voltage source inverter. It is based on a new quantification of the stator flux vector position means a new definition of sectors on the *ab*-plane. The main outcome of this quantification, which takes into account the fact that the voltage vectors available at the output of the faulty inverter have different magnitudes than those of the healthy inverter, is a switching table producing less torque ripple than the table based on the standard sector definition.

Simulations results are presented that demonstrate the continuous operation of the system after the occurrence of a fault as well as its good dynamic response. A frequency analysis shows the torque ripple reduction.

Keywords: reconfigurable control, direct torque and flux control, induction motor drive, fault tolerant voltage source inverter.

1. INTRODUCTION

In certain implementations as fuel-pumps systems, airplanes, steering systems, where the continuous operation of the systems must be ensured, fault tolerant actuators and drives are used to avoid the need of using parallel redundancy to handle faults in this components (Muenchhof et al. 2009).

This work presents a Direct Torque and Flux Control (DTFC) strategy of an induction motor (IM) drive which is reconfigurable under the presence of a fault in the Voltage Source Inverter (VSI).

Among the many fault tolerant topologies for VSIs the switch redundant topology discussed in (Welchko et al. 2005, Fu et al. 1994, Lipo et al. 1997) has been chosen for this work. This topology can handle three different kinds of fault: a short-circuit fault of one switch device, an open-circuit fault of one switch device and a single phase open-circuit. In the presence of a fault, the mentioned topology reconfigurates the VSI which can still generate three phase voltages to feed the IM. The three phase voltages given by the VSI in healthy and faulty operation conditions can be represented as voltage vectors in a stationary reference frame, the so-called *ab*-plane. After the reconfiguration process, only four voltage vectors can be supplied by the VSI instead of the eight obtained in healthy operation conditions. This reduction of control actions produces degradation in the controlled system performance and restrictions in the output power level of the inverter.

DTFC is a vector control strategy that controls directly the stator flux magnitude and the electromagnetic torque of an IM (Takahashi et al. 1988, Tiitinen 1996). Taking into account the desired control actions and the position of the stator flux vector, the control selects an appropriate stator voltage vector from a *Switching Table* (ST), which is constructed in a heuristic way considering a reduced model of the IM.

Torque ripple reduction for DTFC is an important issue of this control scheme that produced significant research activities and numerous results, see (Lai et al. 2004, Lascu et al. 2004, Escobar et al. 2003, and Kang et al. 1998).

Yznaga Blanco et al. (2008) proposed using the switch redundant topology under consideration as part of a fault-tolerant DTFC scheme. The ST used in Yznaga Blanco et al. is based on the standard voltage sectors definition, which results in considerable ripple in the electromagnetic torque. Based on the previous results of (Yznaga Blanco et al. 2008) we propose here a new ST in order to obtain a reconfigured DTFC (ReDTFC) strategy that reduces the torque ripple. This new ST is constructed observing the influence of the new voltage vectors (resulting after the post-fault inverter reconfiguration) on the stator flux magnitude and torque with respect to the position (angle) of the stator flux vector.

The paper is organized as follows: Section II presents the fault tolerant VSI topology and a ReDTFC strategy proposed in (Yznaga Blanco et al. 2008). Section III shows the reasoning followed to obtain the new ST of the proposed ReDTFC. This ST optimizes the application of the space voltage vectors available in the faulty inverter taking into account their projections on a reference frame rotating at stator flux speed (Bertoluzzo et al. 1999). Section IV presents some simulations that demonstrate the continuous operation of the system as well as its good dynamic response. Section V presents conclusions and future work.

2. PREVIOUS RESULTS

2.1 Fault tolerant inverter

There are many different fault tolerant topologies for an AC motor drive. The Switch Redundant topology presented in (Welchko et al. 2005, Fu et al. 1994, Lipo et al. 1997) and depicted in Fig 1 is used here. This topology can handle three different kinds of fault: a short-circuit fault of one switch device, an open-circuit fault of one switch device and a single phase open-circuit. The last kind of fault is not treated in this work.

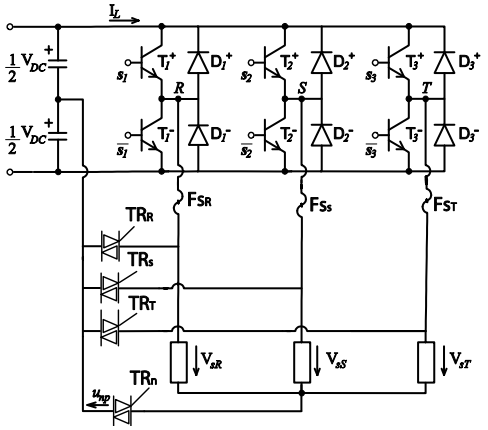

Fig. 1. Schematic circuit of the fault-tolerant VSI.

The switch redundant topology provides a good fault tolerant capability at low cost due to the few additional electronic components employed. Indeed, in addition to the basic inverter, it incorporates only four Triacs and three fast acting fuses (Welchko et al. 2005).

When a short-circuit switch fault is detected, for example in *phase R*, the TR_R is triggered and the voltage over the fuse F_R provokes a high current which blows it. The resulting configuration of the inverter is represented in Fig. 2.

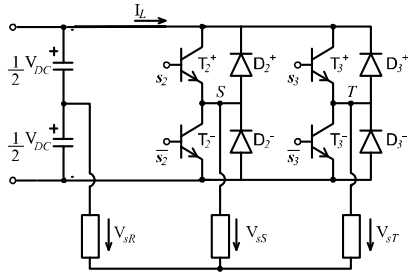

Fig. 2. Schematic circuit after a fault in the *phase R*.

In this work is assumed that a fault detection algorithm detects which component is in faulty condition and perform the triggers in order to isolate the fault.

Equations (1) represent the output voltages of the VSI in terms of the switches states S_i (with $i = R, S, T$). In absence of failure they can take the values *0* or *1* depending on whether the lower switch or the upper switch is in conduction, respectively. When a fault occurs, after the reconfiguration process, and due to the fact that the phase terminal of the stator is connected to the middle point of the DC bus, the model of the VSI can be represented as a value $S_i=0.5$ (with $i=R, S, T$).

$$\begin{aligned} u_{Rn} &= \frac{u_{dc}}{3}(2S_R - S_S - S_T) \\ u_{Sn} &= \frac{u_{dc}}{3}(2S_S - S_T - S_R) \\ u_{Tn} &= \frac{u_{dc}}{3}(2S_T - S_S - S_R) \end{aligned} \tag{1}$$

For example, under a fault in the leg R of the inverter, a reconfiguration mechanism is started and the phase voltages are calculated as:

$$\begin{aligned} u_{Rn} &= \frac{u_{dc}}{3}(1 - S_S - S_T) \\ u_{Sn} &= \frac{u_{dc}}{3}(2S_S - S_T - 0{,}5) \\ u_{Tn} &= \frac{u_{dc}}{3}(2S_T - S_S - 0{,}5) \end{aligned} \tag{2}$$

Evaluating (2) with the possible combinations of the switches state values, ($S_T=1$, $S_T=0$, $S_S=1$, $S_S=0$), we obtain the four voltage vectors previously mentioned. The voltage vectors are different depending on which leg is faulty as it is shown in Fig. 3.

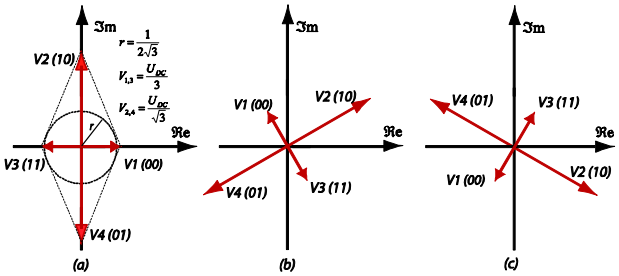

Fig. 3. Voltage Vectors for a fault in the*: (a) R-, (b) S-, (c) T-* inverter leg.

The first harmonic amplitude obtained with the new VSI configuration has half the amplitude of that given by the healthy VSI, represented by the maximum circumference inscribed in the diamond depicted by the new voltage vectors, Fig. 3. This lost of voltage capabilities produces lost of performance of the induction motor, i.e., the motor has to enter in field weakening operation at half rated speed for rated load.

2.2 Direct Torque and Flux Control

This subsection gives a brief description about the principles of the standard Direct Torque and Flux Control scheme (Tiitinen 1996, Depenbrok 1988, Takahashi et al. 1986,).

Fig. 4 shows a schematic block diagram of standard DTFC induction motor drive fed by VSI (Vas 1998). As can be seen from this figure, the DTFC drive has two control loops. One corresponds to a stator flux magnitude and the other one to the electromagnetic torque. Each control loop has a hysteresis comparator that indicates which control action must be performed (to increment or to decrement the magnitudes of stator flux and torque). With these desired control actions and the position of the stator flux vector, a ST is made that outputs the optimum voltage vector to be applied to the motor. The construction of the ST is based on the dynamic equations of the stator flux and electromagnetic torque.

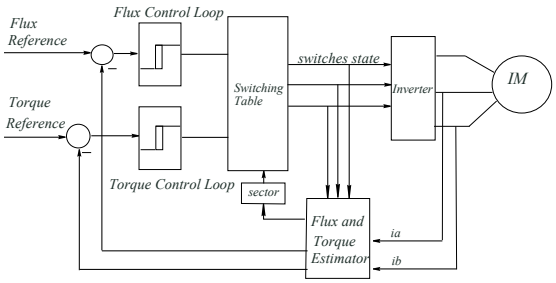

Fig. 4. Schematics of stator flux based DTFC induction motor drive with VSI.

The dynamics of the stator flux vector $\overline{\lambda_s}$ is:

$$\dot{\overline{\lambda_s}} = \overline{V_s} - \overline{i_s} R_s \tag{3}$$

where $\overline{V_s}$ is a voltage vector, $\overline{\imath_s}$ is the stator current vector and R_s is the stator resistance. Neglecting the voltage drop in the stator resistor R_s, the voltage $\overline{V_s}$ modifies directly the dynamics of the stator flux as follows:

$$\overline{\Delta \lambda_s} = \overline{V_s} \Delta T \tag{4}$$

From (4) we observe that the stator flux can be controlled with the appropriate selection of the voltage vector, i.e., the stator flux increment is proportional to the applied voltage vector and the time interval it is applied.

The expression of the electromagnetic torque in terms of the stator and rotor flux vectors is:

$$\tau_{em} = \frac{3}{2} n_p \frac{L_m}{\sigma L_s L_r} \left|\overline{\lambda_r}\right| \left|\overline{\lambda_s}\right| sin(\delta) \tag{5}$$

Where n_p is the number of poles pair of the induction machine, L_s and L_r are the stator and rotor inductance, L_m is the magnetization inductance, δ is the angle between rotor and stator flux vectors, σ is the total leakage factor.

If we consider a generic reference frame *dq* rotating at synchronous speed and the *d* axis aligned with the rotor flux vector, the dynamic relationship between the stator flux and the rotor flux can be considered as a first order delay. So, during a period of time ΔT short with respect to the rotor time constant, the rotor flux can be considered constant regarding variations in the stator flux.

Then, from (5) we see that the instantaneous electromagnetic torque can be controlled modifying the angle δ, provided the stator flux is maintained constant in magnitude. So, an adequate stator voltage vector must be imposed to the induction motor to keep the stator flux magnitude constant and rotate the stator flux vector to a desired position δ.

The selection of the adequate voltage vector depends on the position of the stator flux vector. Standard DTFC algorithm quantifies this position in 6 sectors in the *ab*-plane where each voltage vector bisects each sector. According to this quantification of the complex *ab*-plane (see Fig. 5), an optimal voltage switching table is defined (when $\overline{\lambda_s}$ rotates counterclockwise, see Table 1 (Takahashi et al. 1986)).

In Table 1 a *1* in the columns of stator flux or torque indicates that this magnitude needs to be increased while a *0* indicates that the magnitude needs to be decreased.

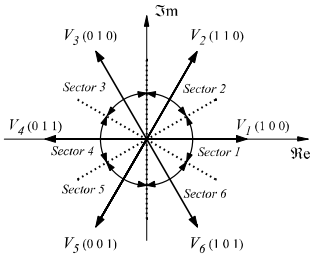

Fig. 5. Voltage vectors for the healthy VSI and sectors.

Table 1. Voltage vector switching table

τ_{em}	λ_s	S1	S2	S3	S4	S5	S6
0	0	V_2	V_3	V_4	V_5	V_6	V_1
0	1	V_3	V_4	V_5	V_6	V_1	V_2
1	0	V_7	V_0	V_7	V_0	V_7	V_0
1	1	V_0	V_7	V_0	V_7	V_0	V_7

2.3 Previous ReDTFC strategy

This subsection explains some previous results presented in (Yznaga Blanco et al. 2008). In that article four sectors are defined according to the four resulting voltage vectors for a fault in one leg of the VSI. Considering a fault in the R leg, the sectors are defined as the area between two voltages vectors as it is shown in Fig. 6.

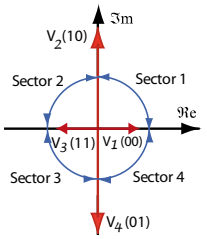

Fig. 6. Sectors and voltage vectors

According to this quantification, the new ST is defined as follows: if the stator flux is in sector 1, the application of the voltage vector V_2 increases the flux magnitude and torque and V_4 decrements both; the application of V_1 increases the flux magnitude and decrements the torque while V_3 produces the opposite effects of V_1. Table 2 shows the ST presented in (Yznaga Blanco et al. 2008).

Table 2. Fault voltage vector switching table (Yznaga Blanco et al. 2008)

τ_{em}	λ_s	S1	S2	S3	S4
0	0	V_4	V_1	V_2	V_3
0	1	V_1	V_2	V_3	V_4
1	0	V_3	V_4	V_1	V_2
1	1	V_2	V_3	V_4	V_1

Due to the fact that the faulty configuration cannot provide null voltage vectors, active vectors are applied to reduce torque. These control actions may produce a non desirable decrease of torque. Besides that, we see from Fig. 6 that the voltage vectors have different modulus, in contrast with those of the healthy configuration.

The effect on τ_{em} of a fault in the *R* leg at time *T=1.2 sec* is shown in Fig. 7, obtained by simulation with a load torque

τ_l=*30 Nm* and ω=*50 rad/sec*. After the fault occurrence a great magnitude of ripple is present in the electromagnetic torque at steady state. This ripple may cause non desirable response of the rotor speed if, for example, a mechanical load is dynamically coupled to the IM.

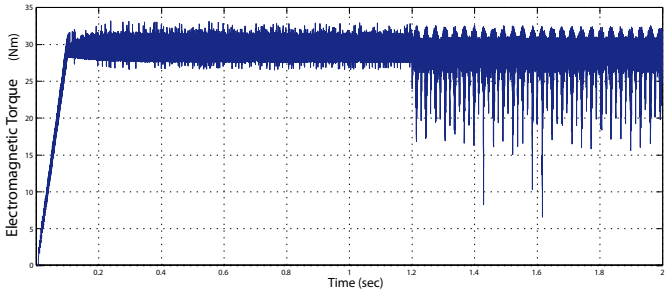

Fig. 7. Electromagnetic torque response.

To better understand the cause of this ripple, Fig. 8 shows the electromagnetic torque (in blue), the stator flux magnitude (in black) and the position of the stator flux quantified in sectors (in red). It can be noted that the electromagnetic torque and the stator flux are scaled, by 1/5 and 4 respectively, in order to make their magnitudes comparable in the figure.

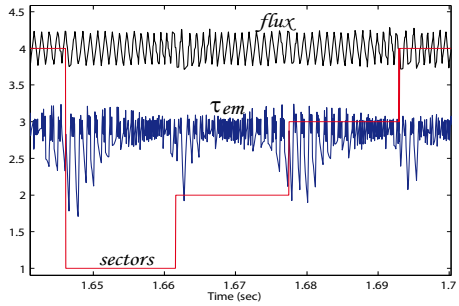

Fig. 8. In blue, zoom of scaled electromagnetic torque; in red, sectors defined in Fig 7; in black, stator flux magnitude.

Fig. 8 shows that the ripple peaks appears when the flux vector is at the transition zone between two sectors defined in Fig. 6. This situation suggests that the voltage vectors given by the ST do not accomplish the desired control action because their influence is not uniform along the entire sector. For example, when the stator flux is leaving *sector 4* and entering *sector 1*, the influence of V_3 increasing the torque is minimum. Moreover, the ripple magnitude is bigger than the hysteresis band of the torque control loop comparator.

The control action proposed by the switching table only can maintain the flux in the limits of the corresponding hysteresis band and its action on the torque cannot compensate the influence of the electromotive force that tends to decelerate the motor. This situation changes when the flux vector achieves the centre of the *sector 1* and starts again at the end of this sector. We can conclude that at the transitions between sectors the drive is commanded only by the flux control loop.

The simulation depicted in Fig. 8 was performed with the control scheme shown in Fig. 4, at rated stator flux and rated load torque.

The behaviour of the control scheme suggests the possibility to modify the control actions to reduce torque ripple. For this purpose it is necessary to know the effects of each voltage vector on the stator flux magnitude and the electromagnetic torque along the corresponding sector. To perform this analysis we use the results in (Bertoluzzo et al. 1999).

3. PROPOSED ReDTFC STRATEGY

To improve the performance of the ReDTFC strategy presented in (Yznaga Blanco et al. 2008) a new ST is introduced here, which is obtained taking the projections of the reconfigured-VSI voltage vectors on a rotating *dq* reference frame whose *d* axis is aligned with the stator flux vector. The effect of the voltage vectors *dq* components on the stator flux magnitude and the electromagnetic torque are given in (6) (see (Bertoluzzo et al. 1999) for its derivation), where λ_{dsr} is the *d* component of the rotor flux referred to the stator, $\omega_{\lambda s}$ is the rotational speed of the stator flux vector.

$$\begin{aligned}\Delta\lambda_s &= \Delta T\left(V_{di} - R_s i_{ds}\right)\\ \Delta\tau_{em} &= \frac{3}{2} n_p \frac{1-\sigma}{2\sigma L_s}\lambda_{dsr}\Delta T\left(V_{qi} - R_s i_{qs} - \omega_{\lambda s}\lambda_s\right) + \frac{\tau_{em}}{\lambda_s}\Delta\lambda_s\end{aligned} \quad (6)$$

It can be seen from (6) that the *d* component of the voltage vector, V_{di}, influences directly the stator flux amplitude, and the *q* component, V_{qi}, influences the torque variation. So, projecting the voltage vectors onto a rotating reference frame aligned with the stator flux vector, it is possible to know the contribution of each one at different positions of the stator flux, see Figure 9.

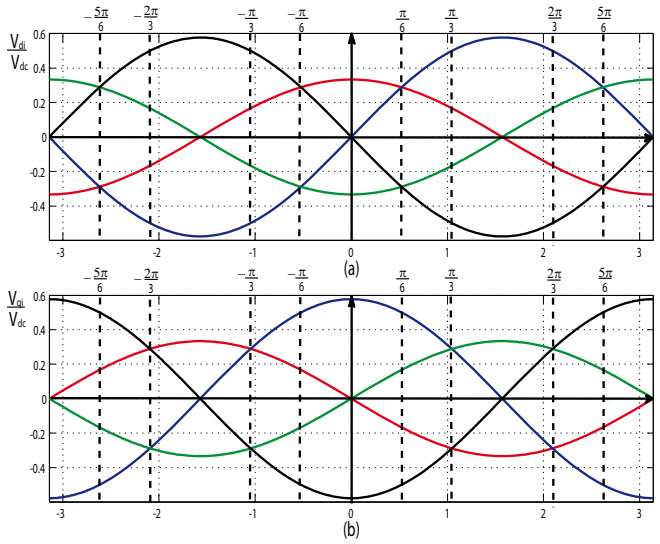

Fig. 9. Normalized Voltage Vector Projection onto: (a) *d* axis, (b) *q* axis. Red, V_1; blue, V_2; green, V_3; black, V_4.

From Fig. 9b we note that the application of V_3 when the stator flux phase is around *0* degrees (begin of sector 1 end of sector 4) produces a decrement in torque instead of an increment, i.e., the voltage vector do not perform the correct control action defined according to Table 2. This phenomenon is repeated in all the transition regions between two sectors. For example, in the transition between sector 1 and *sector 2* vector V_4 does not perform the expected increment of torque.

The behaviour of the voltage vectors, observed in Fig. 9, indicates that it is possible to define some transition sectors. At the new transition sector we propose to apply different

control actions, that overcome the drawbacks above mentioned. According to this analysis, eight sectors are defined; they are delimited with dotted vertical lines in Fig. 9 (a) and (b). *Sector 1* is defined between the vertical lines placed at angles $\frac{\pi}{6}$ and $-\frac{\pi}{6}$. The first one coincides with the intersections of the voltage vectors V_1V_2 and V_3V_4 in Fig. 9 (a) and the other one coincides with the intersection of V_1V_4 and V_2V_3. Between these vertical lines the influence of each voltage vector is clearly determined. For example, V_1 increases the stator flux magnitude whereas V_3 decreases it (see Fig. 9 (a)). Note that the influences of these voltage vectors in the electromagnetic torque are poor due to its low magnitude (see Fig. 9 (b)). The vertical lines are placed at the angle of intersection of two component voltage vectors.

The new quantification of the *ab*-plane is shown in Fig. 10.

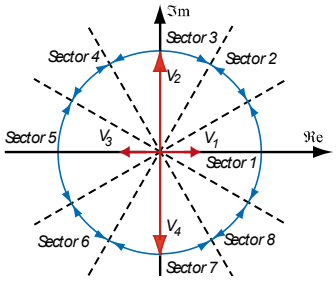

Fig. 10. Sector quantification in ab-plane for a fault in leg *R*.

A new ST is now proposed with the new quantification of the stator flux vector position as follows: in *sector 1*, called transition sector as it coincides with a transition in the previous discrimination, V_2 is applied in order to increase the torque because its influence is always positive (see Fig. 9b); to decrease the torque and increase the flux, V_1 is applied (its influence on the stator flux magnitude is always positive, see Fig. 9 (a); to decrease torque and flux, V_3 is applied (its influence on the stator flux magnitude is always negative, see Fig. 9 (a) and (b)). V_4 is never applied in *sector 1* because it has a great magnitude and the torque reduction will be drastic. In the remaining transition sectors the voltage vectors are chosen following the criteria explained above. In sectors 2, 4, 6 and 8 the influence of each component is clearly determinate, so the voltage vectors are chosen like in section (2.3). Table 3 shows the new fault voltage vector ST.

Table 3. Fault voltage vector ST

τ_{em}	λ_s	S1	S2	S3	S4	S5	S6	S7	S8
0	0	V_3	V_4	V_4	V_1	V_1	V_2	V_2	V_3
0	1	V_1	V_1	V_2	V_2	V_3	V_3	V_4	V_4
1	0	V_2	V_3	V_3	V_4	V_4	V_1	V_1	V_2
1	1	V_2	V_2	V_3	V_3	V_4	V_4	V_1	V_1

4. SIMULATIONS

In this section some simulations results are presented in order to show the performance improvement of the reconfigured control strategy presented in this work. The simulations were performed using Matlab/Simulink with the toolbox developed in (Felicioni et al. 2002). We compare the reconfigurable control strategy proposed here and with that of Section 2.3 (Yznaga Blanco et al. 2008). The induction motor chosen for simulation has the following parameters: R_r=*0.39923Ω*, R_s=*1.165Ω*, *J=0.0812Nm*, L_s=*0.13995H*, L_r=*0.13995H*, L_m=*0.13421H, and* n_p=*2*. To make the simulations more realistic a PI controller was added to close a speed control loop. The switching sampling period used here is T_s=*0.1ms* and estimators compute the stator flux and torque.

The simulation scenario is as follows. The rotor speed reference starts at time zero as a ramp, remains constant after reaching the reference value, and later decreases, again as a ramp, to half its previous value. A load torque of τ_l=*30 Nm* is applied to shown the control performance to reject disturbances.

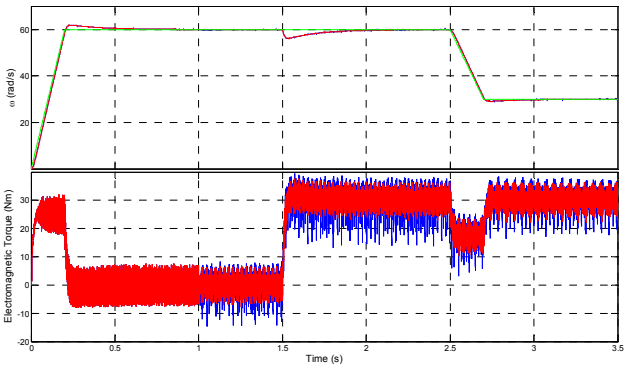

Fig. 11. Dynamic response of the rotor speed and the electromagnetic torque. In red, with the control strategy proposed here; in blue, with the control strategy proposed in (Yznaga Blanco et al. 2008). In green, speed reference.

Fig. 11 shows the dynamic response to a fault occurred in the R leg at time *T=1sec* ω_{ref}*=60 rad/sec*. Fig. 11 shows the good response of both control strategies to reject load torques (applied at *T=1.5sec*) and to follow the rotor speed reference, even after the fault occurrence. Also, it can be noted that the torque ripple is reduced dramatically by the new strategy, as it was predicted previously, especially at high speed, where the action of the electromotive force is strong enough to decelerate the motor (Bertoluzzo et al. 1999).

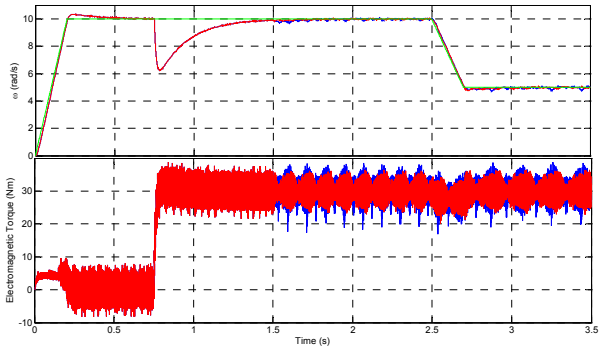

Fig. 12. Dynamic response of the rotor speed and the electromagnetic torque. In red, with the control strategy proposed here; in blue, with the control strategy proposed in (Yznaga Blanco et al. 2008). In green, speed reference.

Fig. 12 shows the dynamic response to a fault in the *R* leg at time *T=1.5 sec* when the rotor reference speed is ω_{ref} *=10 rad/sec*. It can be noted from this figure that with the control strategy proposed here the ripples in the rotor speed and in

the electromagnetic torque are reduced. Moreover, after a fault, the amplitude of the ripple is comparable with the amplitude before the fault. This conclusion is also supported by the frequency analysis (FFT) shown in Fig. 13, where a remarkable reduction can be observed in a frequency interval around 850 Hz. Table 4 shows the RMS values calculated over 1000 points obtained from simulations test of Fig 11 and Fig 12 between 2.4 and 2.5 sec.

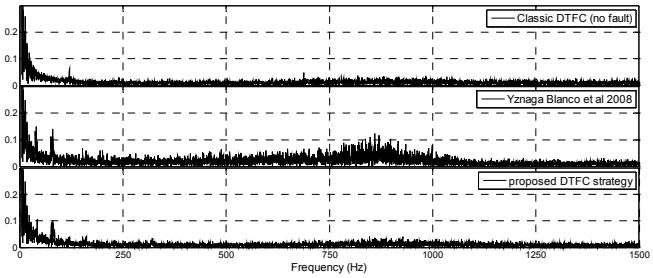

Fig. 13. Fast Fourier Transform of the electromagnetic torque signal. Top, classic DTFC (no fault); middle, DTFC strategy proposed in(Yznaga Blanco et al. 2008); bottom, DTFC strategy proposed here.

Table 4. RMS values

ST proposed in	Simulation Fig. 11		Simulation Fig. 12	
	RMS_ω	RMS_τ_{em}	RMS_ω	RMS_τ_{em}
Yznaga Blanco	0.066	5.176	0.044	3.543
Here	0.045	3.334	0.030	2.581

5. CONCLUSIONS

In this work a ReDTFC strategy for induction motors has been proposed. It works in presence of some faults in the VSI driving the motor and aims at reducing the torque ripple under fault conditions. Analyzing the effects of the voltage vectors (with respect to the stator flux position) on the stator flux magnitude and torque, a new discretization of the flux vector position has been defined that allows to propose a new switching table. With this new table and a very small amount of extra computation (only the new sectors), it is possible to keep the amplitude of the torque ripple in faulty conditions almost the same as in healthy condition. This characteristic allows to improve the performance of the controlled system with respect to an existing reconfigured switching table. The mentioned reduction of torque ripple produces a higher commutation frequency of the inverter switches, with the sample frequency of the controller as the upper limit.

ACKNOWLEDGMENTS

The authors wish to thank CONICET (the Argentine National Council for Scientific and Technological Research), ANPCyT (Argentine National Agency for Scientific and Technological Promotion), under project PICT 2008-0650 and SeCyT-UNR (the Secretary for Science and Technology of the National University of Rosario) for their financial support.

REFERENCES

Bertoluzzo M. Buja G. and Menis R. (1999). "Analytical formulation of the direct control of induction motor drives". In IEEE-Int. Symposium. Industrial Electronics, pages Ps14–Ps20, Bled, Slovenia, 1999.

Depenbrok M. (1988). "Direct self-control (dsc) of inverter-fed induction machine". IEEE Trans. on Power Electronics., 3:420-429.

Escobar G. Stankovic A. M. Galván E. Carrasco J. M. and Ortega R. (2003). A family of switching control strategies for the reduction of torque ripple. IEEE Transaction on Control System Technology, 11(6):933–939, Nov. 2003.

Felicioni F. Pérez T. Molina H. and Junco S. (2002). "Simudrives: A Tool for Computer-Aided Simulation of Electrical Drives and Motion Control Systems". XVIII Congreso Argentino Control Automático, AADECA 2002, 2-4 Sept. 2002, Buenos Aires, Argentina.

Fu J. and Lipo T. (1994). "A strategy to isolate the switching device fault of a current regulated motor drive," in Conf. Rec. IEEE IAS Annu. Meeting, vol. 2, pp. 1015–1020.

Kang J. and Sul S. (1998). Torque ripple minimization strategy for direct torque control of induction motor. In 33rd Annual Meeting Industrial Applications Soc., IEEE-IAS'98, Oct. 98, pages 546–551, St. Louis, USA.

Lai Yen-Shin, Wang Wen-Ke, and Chen Yen-Chang. (2004). Novel switching technique for reducing the speed ripple of AC dives with direct torque control. IEEE Transaction on Industrial Electronics, 51(4):768– 775

Lipo T. Liu T. and Fu J. (1997). "A strategy for improving Reliability of Field-Oriented Controlled Induction Motor Drives". IEEE Transaction on Industry Applications, vol. 29, no. 5, pp. 910-918.

Lascu C. Boldea I. and Blaabjerg F. (2004). Variable-structure direct torque control- A class of fast and robust controllers for induction machine drives. IEEE Transaction on industrial electronics, 51(4):785–792, August 2004.

Muenchhof M. Beck M. and Isermann R. (2009). Fault-tolerant actuators and drives-Structures, fault detection principles and Applications. *Annual Reviews in Control*. Volume 33, pages 136–148

Takahashi I. and Noguchi T. (1986). "A new quick response and high–efficiency control strategy of an induction motor". IEEE Transaction on Industry Applications, 22:820-827.

Tiitinen P. (1996). "The next generation motor control method, DTC direct torque control". Proceedings of the 1996 International Conference on Power Electronics, Drives and Energy Systems for Industrial Growth, vol.1 pp 37-43.

Vas P. (1998) *Sensorless vector and direct torque control*. Chapter 4. Oxford Press.

Welchko A, Lipo T. A, Jahns T. M and Schulz S. E. (2005). "Fault Tolerant Three-Phase AC Motor Drive Topologies: A Comparison of Features, Cost and Limitations" IEEE Transaction on Power Electronics, vol. 19, no. 4, pp. 1108-1116.

Yznaga Blanco I. Dan Sun. and Yi-kang He. (2008). "Study on inverter fault-tolerant operation of PMSM DTC". *Journal of Zhejiang University SCIENCE A*.Vol.9 No.2. 2008